Wide-scale evolution of magnetization distribution in ultrathin films

M. Kisielewski,[1] A. Maziewski,[1] T. Polyakova,[2] and V. Zablotskii[2,3]
[1]*Institute of Experimental Physics, University of Białystok, Lipowa 41, 15-424 Białystok, Poland*
[2]*Donetsk National University, 83055 Donetsk, Ukraine*
[3]*Institute of Physics ASCR, Na Slovance 2, 18221 Prague 8, Czech Republic*
(Received 17 July 2003; revised manuscript received 27 January 2004; published 27 May 2004)

We show, combining simulations and analytical study, the evolution of magnetization distributions in ultrathin film with in-plane fields ($H_{\|}$) and changes of magnetic anisotropy characterized by the quality factor, Q. Reconstruction of the distributions and their new types near Q or $H_{\|}$-induced reorientation phase transitions, from a domain structure (DS) with perpendicular magnetization into a state with in-plane magnetization, are reported. Sinusoidal-like DS exist for $H_{\|}$ larger than the anisotropy field and for $Q<1$. A minimal $8\pi l_{\mathrm{ex}}$ DS period is predicted (l_{ex} is the exchange length).

DOI: 10.1103/PhysRevB.69.184419 PACS number(s): 75.70.Kw, 75.30.Gw

I. INTRODUCTION

The physics of domains in bulk materials and micron-sized films seem to be well understood.[1] But domain patterns of ultrathin films exhibit many new features: unusually sharp thickness dependence of domain sizes,[2,3] disordering and topological reconstruction,[4] inverse ''melting'' phenomenon,[5] strong reconstruction of magnetization distribution in domains related to structural transition,[6] etc. which are of great interest and essential for an understanding of fundamental physics. Generally one can expect ultrathin film in a practically monodomain state—large magnetic domains with geometry determined mainly by coercivity rather than magnetostatic forces. However, domain size drastically decreases down to a submicrometer scale while approaching the reorientation phase transition (RPT). The evolution of magnetic domain structures (DS) and the properties of nanoscaled domains are still an open problem.

RPTs can be driven by either magnetic anisotropy changes or the magnetic field.[2,3] The tuning of anisotropy is realized by different means, changing, e.g., (i) magnetic film thickness, d,[7] (ii) temperature;[8–10] (iii) buffer morphology, roughness,[11–13] (iv) structure of the cover layer;[14–16] (v) composition;[17] (vi) surface-interface roughness.[18] Two parameters are usually used to describe equilibrium domains in a sample: (i) the quality factor $Q=K_1/2\pi M_S^2$, the relation of uniaxial anisotropy to demagnetization energy and (ii) the exchange length $l_{\mathrm{ex}}=[A/(2\pi M_S^2)]^{0.5}$, where A is the exchange constant and M_S is the saturation magnetization. Shape anisotropy modifies the quality factor as the effective factor $Q-1$ for an infinite homogenously magnetized film. When analyzing Q dependent changes of magnetic ordering, regardless of the mechanisms driving Q, one should expect 3D-magnetization distribution. The transition between a closed DS or a partially closed DS to an open DS has been found for thin film increasing Q slightly above 1.[1,19] 2D or 1D magnetization distribution is expected for an ultrathin film. 1D-distributions have been analytically treated with different approaches: (i) stripe DS with negligible thin domain walls (DW),[1,20] (ii) 2 or 3 parametrical models with profiles described by the Jacobi sine function,[21,22] (iii) a cosine-series expansion profile,[23] (iv) DS with a linear DW profile;[24] (v) a 5-parameter model with cosine DW profile;[25] (vi) DS taking into account the distribution of discrete magnetic moments.[26] However, these models are not sufficient to describe the wide range of DS evolution.

The present paper aims to describe the evolution of magnetization distribution and stripelike DSs under changes of Q or $H_{\|}$ in a wide range. We combine analytical approaches and micromagnetic simulations (OOMMF software[27] was used). In Sec. II, we analyze stripe domain size at zero magnetic field, far from the RPT, taking into consideration different models as well as simulations for calculating domain wall energy. A procedure for estimating domain size is proposed. Magnetization distribution evolutions induced by magnetic in-plane applied field and magnetic anisotropy changes are studied in Secs. III and IV, respectively. In Sec. V domains in infinite films close to the RPTs are analytically described in the framework of the sinusoidal model.

II. STRIPE DOMAINS AT ZERO FIELD

In this section our goal is to calculate zero-field domain periods by using different expressions for the density of DW energy. To describe DS far from the RPT, we utilize the Kooy-Enz model of stripe domains with negligible DW width, $\delta_w \ll p$, where p is the stripe period.[1,28] The thickness dependence of the stripe domain period, $p(d/l_c)$ [where $l_c=\sigma_w/(4\pi M_z^2)$ is the characteristic length, σ_w is the DW energy consisting of exchange, anisotropy, and demagnetization energy terms, and M_z is the magnetization component normal to the film] has been described as infinite series[28] which are slowly convergent or as transcendent Lerch's functions.[29] Two useful approximations of this function are given by: (i) $p/l_c=2(d/l_c)\exp[1+(\pi a/2)+(\pi l_c/d)]$, where $a=-0.666$ for $d/l_c \ll 1$ (Ref. 20) or (ii) $p/l_c=c(d/l_c)^m \exp[b/(d/l_c)]$, where $b=3.0613$, $c=2.09513$, and $m=0.85498$; for $0.25<d/l_c<7.5$ the accuracy is better than 4%.

Due to the very sharp dependence of the DS period on d/l_c,[1,20,29] exact knowledge of σ_w plays a crucial role. However, there is a problem with how to precisely determine σ_w, taking into consideration the demagnetizing effect. Obviously, σ_w should follow the relation: $\sigma_B=4(AK_1)^{1/2}>\sigma_w$

TABLE I. Domain wall energy and stripe period analysis performed for the 1 nm Co film (Ref. 2).

	"Bulk" DW	Fully demagnetized DW	Partially demagnetized DW	DW obtained from micromagnetic simulations
Wall energy	0.0190 J/m^2	0.0099 J/m^2	0.0124 J/m^2	0.0121 J/m^2
DS period	30 m	3.6×10^{-4} m	6.5×10^{-3} m	4.74×10^{-3} m

$>\sigma_{\text{eff}}=4[A(K_1-2\pi M_S^2)]^{0.5}$ determined by σ_B—energy of the classical "bulk" DW—regardless of the demagnetization contribution, and the fully demagnetized σ_{eff} one with an effective anisotropy constant. Now we deduce an approximate expression for the density of domain wall energy, taking into account the demagnetizing effect. In the ultrathin regime when $d\ll\delta_w$ [where $\delta_w=\pi(A/K_1)^{1/2}$ is *Lilley*'s domain wall width], DW surface density can be written as $\sigma_p=\sigma_B-2\pi M_S^2\langle\sin^2(\varphi)\rangle\delta_m$ [where $\delta_m=2(A/K_1)^{1/2}$ is domain wall width defined from the slope of the *z*-component of magnetization, $M_z=M_S\sin\varphi$ (Ref. 1) and φ is the angle between the magnetization vector and the film plane]. Notice, considering the magnetostatic energy contribution, that it is natural to use a definition of DW width (δ_m) related to surface magnetic poles. Since within the DW the surface pole distribution obeys $\langle\sin^2(\varphi)\rangle=1/2$, we obtain $\sigma_p=\sigma_B-2\pi M_S^2\ (A/K_1)^{1/2}=\sigma_B-\delta_m\pi M_S^2$. It has been shown in Ref. 30 that for very thin films, i.e., in the limit $d\to0$, domain wall width should be renormalized as $\delta=\delta_0(1-1/Q)^{-1/2}$ (δ_0 is the DW width in bulk materials). Using the last expression, one can arrive[2] at

$$\sigma_p=\sigma_B\left(1-\frac{1}{4Q\sqrt{1-Q^{-1}}}\right). \tag{1}$$

We call this the energy of a partially demagnetized wall. Thus, three different expressions for DW energy can be used to calculate the DS periods: σ_B, a nondemagnetized (bulk) wall; σ_{eff}, a fully demagnetized wall; and σ_p, a partially demagnetized wall. Table I shows the results of DW energy and zero-field stripe period calculations obtained by using the above descriptions for ultrathin cobalt film with $d=1$ nm the effective anisotropy field $H_{A\,\text{eff}}=2K_1/M_s-4\pi M_s=6.66$ kOe and $l_{\text{ex}}=3.2$ nm. One can find a huge difference in the stripe domain periods obtained in the frameworks of the above mentioned descriptions (see Table I).

We obtained the precise demagnetization field influence on both magnetization distribution and wall energy by micromagnetic simulations with OOMMF software. The results are shown in Fig. 1 and Table I. From this figure one can see that the simulated wall profile differs from those of bulk and fully demagnetized walls. The simulated DW energy σ_{sim} is very close to the σ_p of the partially demagnetized DW. So, one can recommend using Eq. (1) for estimating DW energy and the domain periods in an ultrathin film far from the RPTs.

III. EVOLUTION OF MAGNETIZATION DISTRIBUTION WITH IN-PLANE FIELD

Now we consider the evolution of magnetization distribution with an applied field varying from $H_\parallel=0$ up to the field at which the magnetization comes down to the film plane.

Let us first discuss this evolution in the framework of classical description.[1] According to the description, one can expect that, by increasing field $H_\parallel$, magnetization rotates to the film plane as $\cos\Theta=H_\parallel/H_{A\,\text{eff}}$, where Θ is measured from the plane of the film and $H_\parallel$ is applied along the *y*-axis (see the inset to Fig. 2). Taking into account the field dependence of the Bloch DW energy[1] and using the Kooy-Enz model,[28] we calculate $p(H_\parallel)$-dependencies (Fig. 2) obtained for both "bulk" and fully demagnetized walls. Typical ultrathin Co sample parameters[2] $d=1$ nm, $H_{A\,\text{eff}}=6.66$ kOe; $l_{\text{ex}}=3.2$ nm are assumed. Comparing $p(H_\parallel)$ and $\delta_w(H_\parallel)$, shown in Fig. 2, we find that DS descriptions based on the assumption $\delta_w\ll p$ are not valid in a wide field region before $H_{A\,\text{eff}}$ because the DW width becomes comparable to p while approaching $H_\parallel$-induced RPT. Thus, in this field region a complicated magnetization distribution is expected because of the demagnetizing effect.

For precise description of the evolution of in-plane field-induced magnetization distribution, micromagnetic simulations were performed [see examples in Figs. 3(A), 3(B), 3(C)]. 3000 cells used in simulations enabled the study of a 3000 nm large sample (with $H_{A\,\text{eff}}=6.66$ kOe; $l_{\text{ex}}=3.2$ nm) [see Fig. 3(E)]. Stripe domain structures with period p_S (N_S domains in 3000 nm) and $m_z=\sqrt{1-(H_\parallel/H_{A\,\text{eff}})^2}$ were assumed for the OOMMF minimization procedure[27] in the starting step. A magnetization distribution characterized by total "sample" energy E_{TOT}, period p, and the amplitude A_0 in

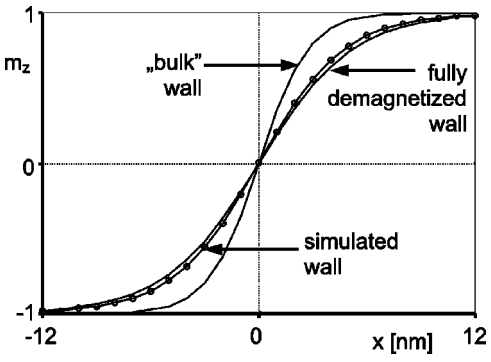

FIG. 1. Zero field magnetization distributions in the following single DWs: "bulk," fully demagnetized, and "realistic," obtained by micromagnetic simulation [the line with circles (○)].

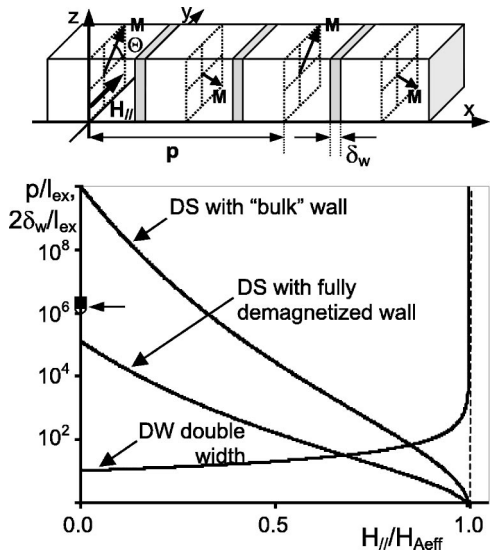

FIG. 2. Field dependencies of (i) stripe DS periods calculated from models neglecting DW width (see the formulas in Sec. II) and taking into consideration domain wall energies σ_B and σ_{eff}; (ii) isolated DW double width $2\delta_w$ determined considering full DW demagnetization. Zero field normalized DS periods calculated with σ_p and σ_{sim} are marked by a full square (■) and an open circle (○), respectively (note: these two symbols overlap and are additionally marked by horizontal arrow). The inset shows DS and field configuration. Calculations were performed for the magnetic parameters of an Au/Co/Au sample (Ref. 2).

the domain center [defined in Fig. 3(C)] was obtained. The distribution with minimal energy was finally chosen [see as an example, Figs. 3(A), 3(B), 3(C)].

Let us now analyze magnetization distributions obtained from simulations [see examples in Figs. 3(A), 3(B), 3(C)]. For fields close to $H_{A\,\text{eff}}$, novel "exotic" $m_z(x)$-dependencies were found which are impossible to predict using current analytical descriptions based on rather simple trial functions [see Figs. 3(A) and 3(B)]. Here one can find peculiarities [marked by vertical arrows in Fig. 3(B)] and a significant increase of the DW width. The distortion—an increase of magnetization amplitude—is easily explained, taking into consideration the decrease of the demagnetization field while approaching both the sample and domain edge, if the DW width is wide enough for a small enough m_z. Qualitatively, demagnetization locally "increases" magnetic anisotropy resulting in an increase in m_z. Increasing $H_\parallel$ up to $H_{A\,\text{eff}}$, the $m_z(x)$ gradually transforms into a sinusoidal-like distribution, shown in Figs. 3(A)–3(C) and Fig. 4. As is seen from Fig. 4, the amplitude A_0 decreases while field increases. But at $H_\parallel \approx H_{A\,\text{eff}}$ the amplitude is still large enough, contrary to the classical theory prediction, so the transition into a monodomain state takes place at $H_\parallel > H_{A\,\text{eff}}$. A further increase of $H_\parallel$ leads to zero m_z in the sample, except in the edge regions. The field dependence of the period, the line in Fig. 5, has been constructed using points taken from simulations—full circles (●)—and calculations based on models[1,20] with DW energy determined from simulations performed for a single DW—open circles (○). Remarkably, the curve starts and ends very close to two analytically determined points: the full square (■)—$p(0)$ calculated with the σ_p and the asterisk (∗)—p^* given by Eq. (7), see below.

IV. EVOLUTION OF MAGNETIZATION DISTRIBUTIONS WITH CHANGES OF ANISOTROPY

Let us now consider DS evolution with changes of Q up to the RPT. The most discussed case is thickness driven RPT caused by $Q(d)$ at zero field. Our consideration is illustrated by ultrathin cobalt in a gold envelope with parameters[16] $Q=(K_{1v}+2^*K_{1S}/d)/2\pi M_S^2$, where $K_{1v}=1.9$ MJ/m^3 and $K_{1s}=0.57$ mJ/m^2. Figure 6 shows the thickness dependence of the DS period and DW width calculated with the Kooy-Enz model and the above $Q(d)$-dependence. Similarly as for $H_\parallel$-induced RPT, here for Q-RPT the classical description falls (DW width becomes comparable to p) far from the RPT, see Figs. 2 and 6. Magnetization distributions simulated for various d are shown in Figs. 7(A)–7(C). It is interesting to note that neglecting higher order anisotropy constants, from the point of view of classical description,[1] one can expect a jump between the perpendicular and in-plane magnetization orientations when $K_{\text{eff}}(d=d_1)=0$. However, the existence of domains and their magnetostatic contribution changes the transition nature to a continuous one. Indeed, it is clearly seen from Fig. 8 that the amplitude gradually decreases when the film thickness approaches the critical thickness d_1. Here a two-step evolution of magnetization distribution can be distinguished. In the first step the DW width increases (resulting at d_1 in the formation of a sinusoidal-like DS, see Fig. 8) while magnetization amplitude only slightly decreases at d_1. In the second step, A_0 decreases, increasing d above d_1. In Fig. 9 the DS period versus thickness is shown by the curve which was constructed in a similar way to the one in Fig. 5: those points given by simulations are represented by full circles (●); calculations based on models[1,20] with DW energy determined from simulations performed for a single DW are represented by open circles (○). Similar to the $p(H_\parallel)$-dependence shown in Fig. 5, the $p(Q)$-curve starts and ends very close to two analytically determined points: the full square (■) shows $p(d)$ calculated with the σ_p and the asterisk (∗) shows p^* given by Eq. (7), see below. It is important to note that sinusoidal domains exist above the RPT thickness ($d>d_1$). Similarly, the domain existence at $H>H_{A\,\text{eff}}$ was described in the previous section.

V. SINUSOIDAL MODEL OF MAGNETIZATION DISTRIBUTION NEAR THE RPT

In order to grasp RPT physics, which is difficult to do using only simulations, we utilize the sinusoidal-like DS model[26] in which the magnetization varies as $m_z(x)=\Theta_0 \sin(2\pi x/p)$ (see domain geometry and the coordinate system in Fig. 10). The total energy of an infinite film, E, is described by the sum of the exchange, anisotropy, Zeeman and demagnetizing energies

$$E=L_y d\int_0^{p/2}\left(A\left(\frac{d\theta}{dx}\right)^2+K_1\sin^2(\theta(x))\right.$$
$$\left.-M_S H_\parallel \sin(\theta(x))\right)dx+E_D, \qquad (2)$$

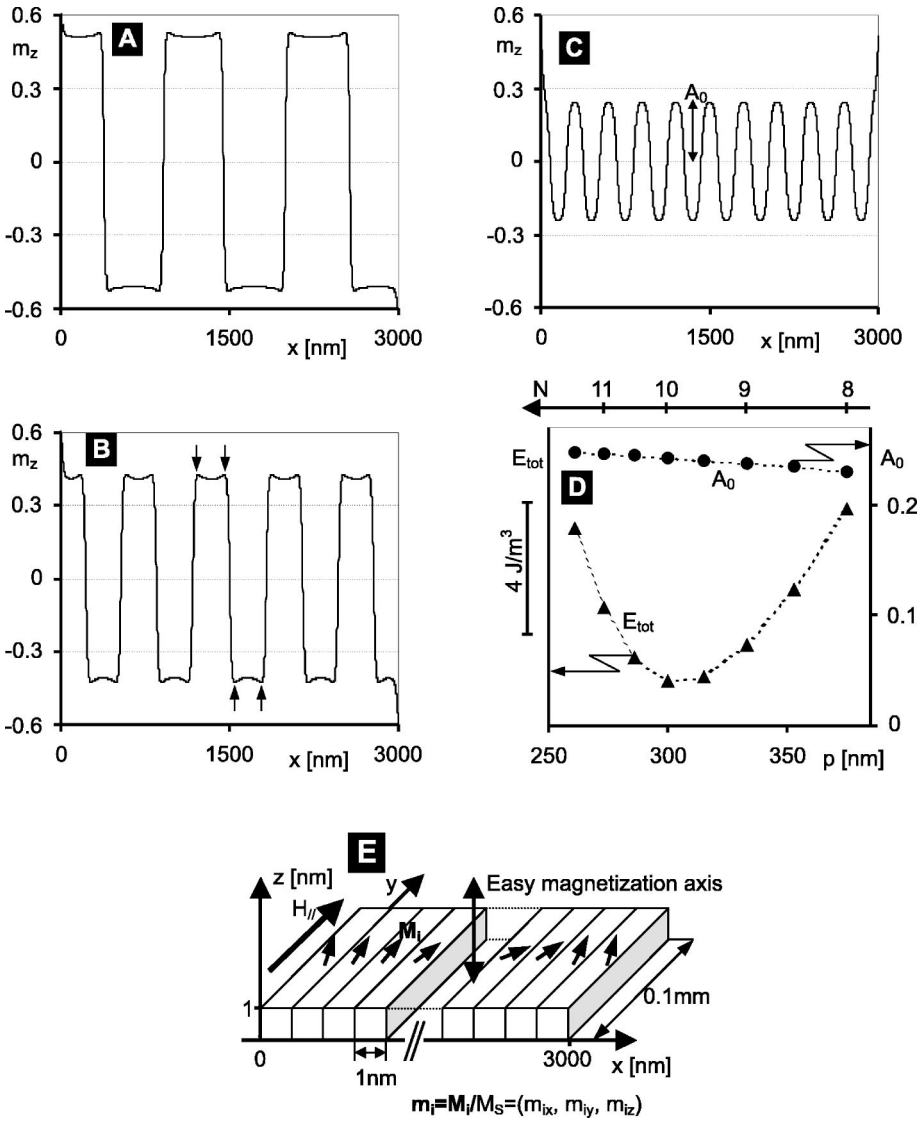

FIG. 3. Magnetization distribution of minimal E_{TOT} in the $1\times3000\times100000\ \mathrm{nm}^3$ sample determined by micromagnetic simulations for in-plane applied fields: (A) $H_{\parallel}/H_{A\,\mathrm{eff}}=0.87$; (B) $H_{\parallel}/H_{A\,\mathrm{eff}}=0.93$ (vertical arrows indicate peculiarities of magnetization distribution, see Sec. III); (C) $H_{\parallel}/H_{A\,\mathrm{eff}}=1.0$. (D) Shows E_{TOT} and A_0 vs p for $H_{\parallel}/H_{A\,\mathrm{eff}}=1.0$ [A_0 is defined in (C); upper scale defines the number N of DS periods in the ''sample'']. (E) Illustrates the geometry of the model used in simulations. Simulations were performed for the magnetic parameters of an Au/Co/Au sample (Ref. 2).

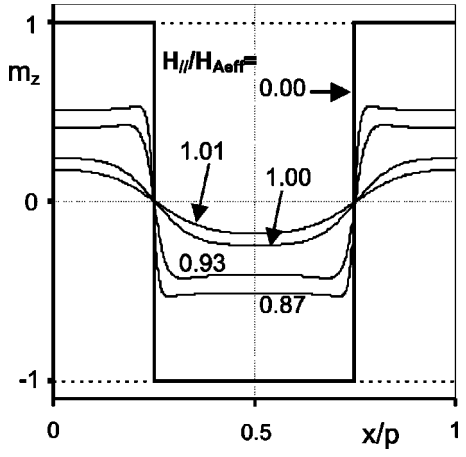

FIG. 4. Simulated magnetization distributions $m_z(x/p)$ determined for different normalized $H_{\parallel}/H_{A\,\mathrm{eff}}$ fields [some of these distributions are shown in larger scale in Figs. 3(A), 3(B), 3(C)]. Simulations were performed for the magnetic parameters of an Au/Co/Au sample (Ref. 2).

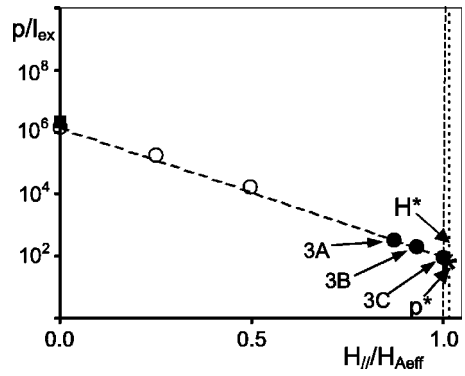

FIG. 5. Field dependence of DS period determined from: simulations (●) and calculations (○) using $p(d/l_c)$ (see formulas in Sec. II) with domain wall energy σ_{sim} obtained from simulations for isolated DW. Full square (■) marks DS period calculated with σ_p. The critical DS period determined from Eq. (7), for the sinusoidal DS at H^* is marked by an asterisk. All periods are normalized to l_{ex}. Simulations were performed for the magnetic parameters of a Au/Co/Au sample (Ref. 2).

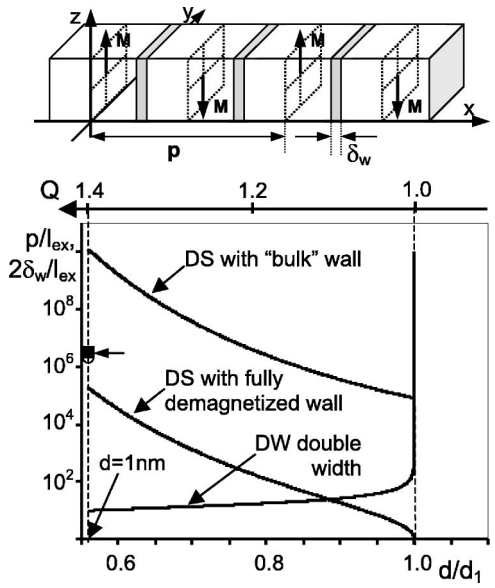

FIG. 6. Thickness (and Q) dependencies of DS period: (i) stripe DS periods calculated from a model neglecting DW width (see formulas in Sec. II) and taking into consideration domain wall energies σ_B and σ_{eff}, (ii) isolated DW double width $2\delta_w$ determined considering full DW demagnetization. Zero field normalized DS periods calculated with σ_p and σ_{sim} are marked by the full square (■) and the open circle (○), respectively (note: these two symbols overlap and are additionally marked by horizontal arrow). Notice, d_1 is the critical RPT thickness determined by $K_{1\ \text{eff}}(d_1)=0$. The inset shows DS configuration. Calculations were performed for the magnetic parameters of an Au/Co/Au sample (Ref. 16).

where L_y is the domain length along domain walls; $\theta(x)$ is the polar angle (a periodical function, with period p, determining the magnetization distribution in the film); E_D represents the demagnetizing energy. For the sinusoidal DS, Eq. (2) can be written as

$$\frac{E_{\sin}}{2\pi M_S^2 l_{\text{ex}}} = Q\frac{d}{l_{\text{ex}}}\left(1-\frac{\Theta_0^2}{2}\right)+\frac{4\pi^2 d l_{\text{ex}}}{p^2}(1-\sqrt{1-\Theta_0^2}) - 4h\frac{d}{l_{\text{ex}}}\frac{E(\Theta_0^2)}{\pi}+\frac{\Theta_0^2 p}{4\pi l_{\text{ex}}}\left(1-\exp\left(-\frac{2\pi d}{p}\right)\right). \tag{3}$$

Here $h=H_{\parallel}/4\pi M_S$ and $E(\Theta_0)$ is the elliptical integral. In the next step we minimize Eq. (3) with respect to amplitude Θ_0 and DS period p. This gives two equations

$$\left(1-\frac{\pi d}{p}\right)-Q+\frac{4l_{\text{ex}}^2\pi^2}{p^2\sqrt{1-\Theta_0^2}}+h=0 \tag{4}$$

and

$$\left(1-\frac{\pi d}{p}\right)\frac{\Theta_0^2}{2}-\frac{\Theta_0^2}{2}\left(1-\frac{2\pi d}{p}+2\left(\frac{\pi d}{p}\right)^2\right) - \frac{8l_{\text{ex}}^2\pi^2}{p^2}(1-\sqrt{1-\Theta_0^2})=0. \tag{5}$$

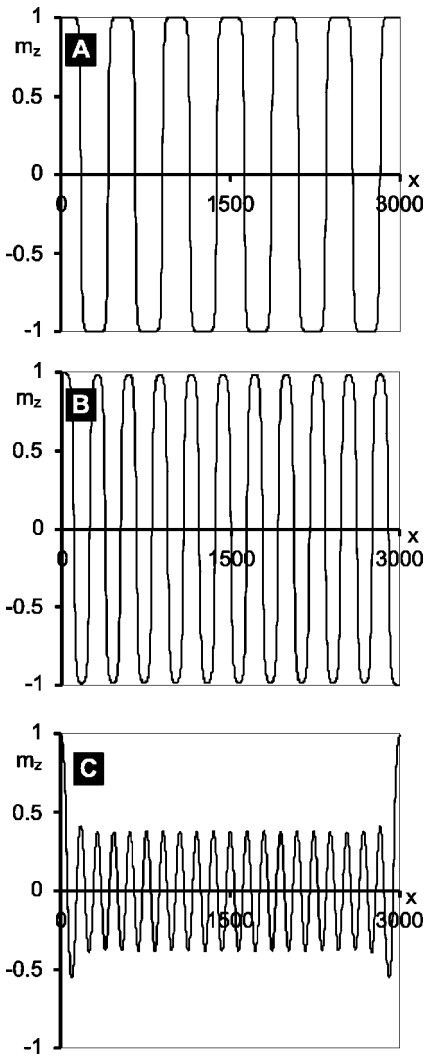

FIG. 7. Zero-field magnetization distributions determined by micromagnetic simulations for different sample thickness: (A) $d/d_1=0.96$; (B) $d/d_1=1.0$; (C) $d/d_1=1.04$ ($d_1=1.79$ nm). Simulations were performed for the magnetic parameters of an Au/Co/Au sample (Ref. 16).

Note, that both the expansion of the elliptical integral into the series with respect to the small parameter Θ_0 and the expansion of the exponential function with respect to $d/p \ll 1$ (both to the second orders) were used to obtain Eqs. (4) and (5). From Eq. (5) the relationship between the domain period (p) and amplitude can be obtained as

$$p=\frac{2l_{\text{ex}}^2\pi\left(8(1-\sqrt{1-\Theta_0^2})+\Theta_0^2\frac{d^2}{l_{\text{ex}}^2}\right)}{\Theta_0^2 d}. \tag{6}$$

When the parameter Θ_0 goes to zero, the DS period approaches its minimal value of

$$\frac{p^*}{l_{\text{ex}}}=\frac{8\pi l_{\text{ex}}}{d}+2\pi\frac{d}{l_{\text{ex}}}. \tag{7}$$

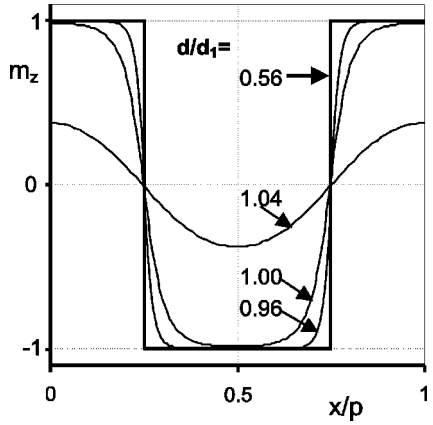

FIG. 8. Magnetization distribution, $m_z(x/p)$ for different normalized sample thickness d/d_1 [some of these distributions are shown in larger scale in Figs. 7(A), 7(B), 7(C)]. Simulations were performed for the magnetic parameters of an Au/Co/Au sample (Ref. 16).

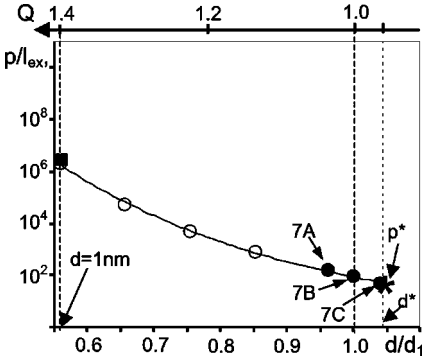

FIG. 9. Thickness (and Q) dependencies of DS period determined from: simulations (●) and calculations (○) using the $p(d/l_c)$ (see formulas in Sec. II) with domain wall energy σ_{sim} obtained from simulations for isolated DW. Full square (■) marks DS period calculated with σ_p. The critical DS period determined for sinusoidal DS at Q^* is marked by the asterisk, $d_1 = 1.79$ nm. All periods are normalized to l_{ex}. Simulations were performed for the magnetic parameters of an Au/Co/Au sample (Ref. 16).

Equation (7) determines the minimal DS period available in an ultrathin film. The period is much smaller than that given by the classical model outside the RPT (see Fig. 2). In Figs. 5 and 9 we marked p^* calculated from Eq. (7). Analyzing Eq. (7), one can deduce that the minimal available DS period is $8\pi l_{\text{ex}}$ at $d = 2l_{\text{ex}}$.

Now we calculate the critical values of anisotropy factor and the magnetic fields (Q^* and H^*) at which the transition from a domain state to the monodomain in-plane state should take place. A sinusoidal domain structure appears, if it leads to a decrease in the system energy, i.e., when $\Delta E = E_{\text{sin}} - E_{\text{in-pl}} < 0$ (where $E_{\text{in-pl}}$ is the energy of the mono-domain in-plane state). So, the critical quality factor and field are determined by conditions: $E_{\text{sin}}(Q^*) = E_{\text{in-pl}}$ and $E_{\text{sin}}(H^*) = E_{\text{in-pl}}$. The following formulas for critical Q^* and H^* were obtained from the energy balance condition of sinusoidal DS and the in-plane monodomain state and Eqs. (3)–(5),

$$1 - Q^* = \frac{H^* - H_{A\,\text{eff}}}{4\pi M_S} = \frac{(d/l_{\text{ex}})^2[2 + (d/l_{\text{ex}})^2]}{2[4 + (d/l_{\text{ex}})^2]^2}. \qquad (8)$$

Qualitatively, Eq. (8) means that the magnetostatic forces of domains shift the RPT, increasing the range of the existing multidomain state. A similar shift in the quality factor, for which sinusoidal-like domains occur in an atomic monolayer, was analytically shown in Ref. 26. The shift, which is equal to that given by Eq. (8), is also found in our simulations (see Figs. 5 and 9): domains are found to exist at $H_{A\,\text{eff}} \leqslant H_{\|} < H^*$ and $d_1 \leqslant d < d^*$ [the critical thickness d^* is defined by $Q(d^*) = Q^*$]. Note, micromagnetic simulations and calculations with Eq. (8) give the same values of the shifts for either the $H_{\|}$ or Q boundaries of the existence of the domains. The periods p^* at both critical points H^* and Q^*, calculated from Eq. (7) [marked by an asterisk (*) in Figs. 5 and 9], are in good agreement with our simulation results. In Refs. 3 and 31, 300–500 nm sized domains were observed in the so-called gray-zone thickness regime—the thickness of the transition from the perpendicular to in-plane magnetization. The gray-zone domains had both out-of plane and in-plane magnetization components, but the angle Θ_0 was unknown. Since Eq. (7) is applicable for small Θ_0, one can only make a qualitative comparison of its results with this experiment. It is satisfactory, that periods (p^*) calculated from Eq. (7) and DS periods given by simulations (Figs. 5 and 9) as well as the observed DS sizes,[31] have the same order of magnitude.

The domain structure transforms into a sinusoidal one under the influence of the increasing in-plane field or decreasing anisotropy. In this sense the sinusoidal DS represents the end point of the evolution of magnetization distributions and helps us to find the boundaries of the existence of domain.

The analysis which we performed started from the initial sample state $d = 1$ nm, $H_{\|} = 0$, see Figs. 2, 5, and 9. We studied magnetization evolution on the $(Q, H_{\|})$-plane in two selected Q and $H_{\|}$ ''directions.'' The evolution for both ''directions'' is very similar close to RPT. There are also some differences: (i) the changes in magnetization amplitude take place in the much wider range of $H_{\|}$ than of Q (or d);[32] (ii) $H_{\|}$ induces only 1D distributions especially for higher fields. It should be stressed here that the analytical results [Eqs. (7) and (8)] were obtained for infinite ultrathin films. In finite samples the equilibrium magnetization distribution is also dependent on the boundary conditions superimposed on the problem and sample geometry. However, for samples of

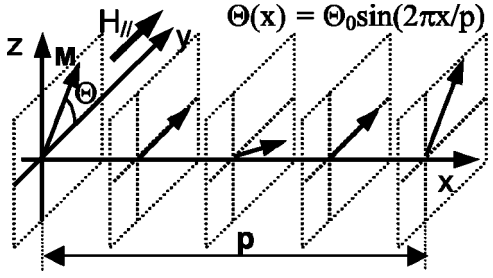

FIG. 10. Magnetization distribution in the sinusoidal model.

large enough lateral sizes the edge effect is small and in the RPT region they may exhibit sinusoidal domains with period defined by Eq. (7).

VI. CONCLUSIONS

In conclusion, for a wide range of Q and $H_{\|}$-changes, the evolution of magnetization distributions in ultrathin films was described with regard to the demagnetizing fields contribution. Our analytical study and simulations bring an understanding of magnetization distribution in wide scale evolution driven by different mechanisms—field, anisotropy changes, etc. We give simple analytical formulas allowing calculations of periods of DS in infinite ultrathin films near and far from RPTs, as well as estimations of domain sizes in the intermediate regions. We show the possibilities for great changes in domain size from practically infinite to hundreds, or even dozens, of nanometers. These changes are available even for a given sample using an in-plane applied field, e.g., see the huge domains and a dense metastable DS ''frozen'' by coercivity in Ref. 2. The nanosized domains are tunable by external fields, Q parameter changes (realized by sample thickness, coverage, roughness, stress, etc.) and magnetic patterning. This is important for general knowledge and for possible applications related to new memory devices, GMR affected by DS, etc. It also opens new directions for experimental and theoretical study of magnetism in the nanometer scale.

ACKNOWLEDGMENT

This work was supported by the Polish State Committee for Scientific Research (Grant No. 4T11B 006 24) and European Commission program ICA1-CT-2000-70018 (Center of Excellence CELDIS).

[1] A. Hubert and R. Schäfer, *Magnetic Domains* (Springer, Berlin, 1998).
[2] M. Kisielewski, A. Maziewski, V. Zablotskii, T. Polyakova, J. M. Garcia, A. Wawro, and L. T. Baczewski, J. Appl. Phys. **93**, 6966 (2003).
[3] M. Speckmann, H. P. Oepen, and H. Ibach, Phys. Rev. Lett. **75**, 2035 (1995).
[4] A. Vaterlaus, C. Stamm, U. Maier, M. G. Pini, P. Politi, and D. Pescia, Phys. Rev. Lett. **84**, 2247 (2000).
[5] O. Portmann, A. Vaterlaus, and D. Pescia, Nature (London) **422**, 701 (2003).
[6] R. Zdyb and E. Bauer, Phys. Rev. B **67**, 134420 (2003).
[7] *Ultrathin Magnetic Structures*, edited by B. Heinrich and J. A. C. Bland (Springer, Berlin, 1994), and references therein.
[8] D. P. Pappas, K. P. Kämper, and H. Hopster, Phys. Rev. Lett. **64**, 3179 (1990).
[9] A. Berger and H. Hopster, Phys. Rev. Lett. **76**, 519 (1996).
[10] R. Sellmann, H. Fritzsche, H. Maletta, V. Leiner, and R. Siebrecht, Phys. Rev. B **64**, 054418 (2001).
[11] P. Poulopoulos, J. Lindner, M. Farle, and K. Baberschke, Surf. Sci. **437**, 277 (1999).
[12] D. M. Schaller, D. E. Bürgler, C. M. Schmidt, F. Meisinger, and H.-J. Güntherodt, Phys. Rev. B **59**, 14516 (1999).
[13] S. P. Li, W. S. Lew, J. A. C. Bland, L. Lopez-Diaz, C. A. F. Vaz, M. Natali, and Y. Chen, Phys. Rev. Lett. **88**, 087202 (2002).
[14] B. N. Engel, M. H. Wiedmann, and C. M. Falco, J. Appl. Phys. **75**, 6401 (1994).
[15] P. Beauvillain, A. Bounouh, C. Chappert, R. Mégy, S. Ould-Mahfoud, J. P. Renard, P. Veillet, D. Weller, and J. Corno, J. Appl. Phys. **76**, 6078 (1994).
[16] M. Kisielewski, A. Maziewski, M. Tekielak, A. Wawro, and L. T. Baczewski, Phys. Rev. Lett. **89**, 087203 (2002).
[17] M. Dreyer, M. Kleiber, A. Wadas, and R. Wiesendanger, Phys. Rev. B **59**, 4273 (1999).
[18] H. Szymczak, M. Rewienski, and R. Żuberek, J. Magn. Magn. Mater. **139**, 151 (1995).
[19] R. Szymczak, Electron Technol. **1**, 5 (1968).
[20] B. Kaplan and G. A. Gehring, J. Magn. Magn. Mater. **128**, 111 (1993).
[21] A. L. Sukstanskii and K. I. Primak, J. Magn. Magn. Mater. **169**, 31 (1997).
[22] A. Marty, Y. Samson, B. Gilles, M. Belakhovsky, E. Dudzik, H. Dürr, S. S. Dhesi, G. van der Laan, and J. B. Goedkoop, J. Appl. Phys. **87**, 5472 (2000).
[23] Sug-Bong Choe and Sung-Chul Shin, Phys. Rev. B **59**, 142 (1999).
[24] G. Castro, G. A. Gehring, and S. J. Robinson, J. Magn. Magn. Mater. **214**, 85 (2000).
[25] A. Berger and R. P. Erickson, J. Magn. Magn. Mater. **165**, 70 (1997).
[26] Y. Yafet and E. M. Gyorgy, Phys. Rev. B **38**, 9145 (1988).
[27] M. Donahue and D. Porter, Object Oriented Micromagnetic Framework, http://math.nist.gov/oommf, free software for micromagnetic simulations.
[28] C. Kooy and U. Enz, Philips Res. Rep. **15**, 7 (1960).
[29] A. Maziewski, V. Zablotskii, and M. Kisielewski, Phys. Status Solidi A **189**, 1001 (2002).
[30] E. Schlömann, J. Appl. Phys. **44**, 1837 (1973).
[31] H. P. Oepen, M. Speckmann, Y. Millev, and J. Kirschner, Phys. Rev. B **55**, 2752 (1997).
[32] In this paper we discuss the simplest case, taking into account only K_1. Considering the K_2 constant: (i) the range of existence of canted magnetization in DS could be extended ($K_2>0$), (ii) the transition character could be changed ($K_2<0$). Canted magnetization in out-of-plane-DS has been recently measured in the whole thickness range in ultrathin FeCo (Ref. 6), where more complicated magnetic anisotropy contributions are expected.